

Articles

Excitation Energy Transfer Rate Constants in meso-meso Linked Zn(II) Porphyrin Arrays with Energy Accepting 5,15-Bisphenylethynylated Zn(II) Porphyrin

Damee Ko, Heeyoung Kim,[†] Jin Hee Park, Dongho Kim,^{*} and Eunji Sim^{†,*}Center for Ultrafast Optical Characteristics Control and [†]Department of Chemistry, Yonsei University, Seoul 120-749, Korea^{*}E-mail: dongho@yonsei.ac.kr, esim@yonsei.ac.kr

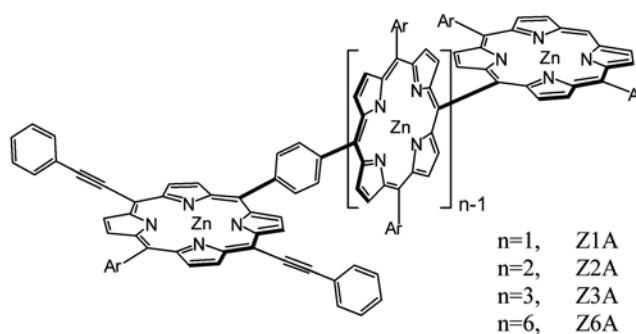
Received June 21, 2005

The excitation energy transfer process occurring in energy donor-acceptor linked porphyrin array system is theoretically simulated using the on-the-fly filtered propagator path integral method. The compound consists of an energy donating meso-meso linked Zn(II) porphyrin array and an energy accepting 5,15-bisphenylethynylated Zn(II) porphyrin, in which the donor array and the acceptor are linked via a 1,4-phenylene spacer. Real-time path integral simulations provide time-evolution of the site population and the excitation energy transfer rate constants are determined. Simulations and experiments show an excellent agreement indicating that the path integration is a useful tool to investigate the energy transfer dynamics in molecular assemblies.

Key Words : Porphyrin, Energy transfer, Path integral, Simulation

Introduction

A photosynthetic bacterium, such as *Rhodobacter Sphaeroides* and *Rs. Molichianum*, maintains its life through highly efficient chain reactions initiated by the absorption of photon at light harvesting antenna complexes.¹⁻³ The light-harvesting complexes are molecular aggregates that consist of peptides, chlorophylls, and carotenoids. Main function of such molecular aggregates is to funnel the energy to the reaction center in which primary charge separation takes place. Therefore, molecular structures can absorb radiation, transform it into electronic energy, and energy storage can be achieved as artificial molecular photonic devices similar to the light harvesting antenna complexes in nature.⁴⁻⁶ Recently, ZnA porphyrin molecular assemblies (Scheme 1) have been successfully synthesized, which have a 5,15-bisphenylethynylated porphyrin acceptor linked via a 1,4-phenylene spacer at the n^{th} meso-carbon of meso-meso linked Zn(II) porphyrin donor array.⁶ The triple bond linkage (ethynylated) at two meso positions of the acceptor porphyrin moiety has elongated π -conjugation pathway leading to the lowering of the excited electronic state of the acceptor. This feature enables ZnA to realize unidirectional energy transfer from photoexcited donor array (Zn) to energy acceptor (A) upon reaching the terminal Zn(II) porphyrin unit attached to A in ZnA through excitation energy migration processes. The absorption spectra of these hybrid porphyrin arrays in the Q-band region are essentially given by the sum of the absorption spectra of meso-meso linked Zn array and A.^{7,8} This feature indicates that electronic interactions in the ground state between Zn and A are weak due to a 1,4-phenylene spacer. Thus, it is possible to excite the donor array selectively by tuning the excitation



Ar = 3,5-dioctyloxyphenyl.

Scheme 1. Molecular structure of ZnA systems.

wavelength to be resonance with the Q-band of the donor array Zn and to observe the excitation energy transfer (EET) within the system using transient absorption spectroscopy.⁶ The transient absorption spectra of ZnA were previously reported by selective excitation of Zn, which revealed that the energy transfer process from initially photoexcited Zn to the ground state A occurs very fast and quantitatively. The EET rate constants were estimated to be $(2.5 \text{ ps})^{-1}$ for Z1A, $(3.3 \text{ ps})^{-1}$ for Z2A, $(15.5 \text{ ps})^{-1}$ for Z3A, and $(21 \text{ ps})^{-1}$ for Z6A, $(63 \text{ ps})^{-1}$ for Z12A, and $(108 \text{ ps})^{-1}$ for Z24A, respectively.

Although the energy transfer processes in ZnA systems have been well-explored experimentally, theoretical studies in such molecular photonic assemblies, however, are still in a rudimentary stage. Although the EET is ubiquitous in photosensitive materials, theoretical interpretation still relies on the theories developed, almost five decades ago, by Förster and Dexter. The Förster's rate equation is based on the Fermi's golden rule, where the perturbation is the

induced dipole-dipole interaction between molecules.⁹ Later, Dexter has adapted the Förster's theory to the case of solids, incorporating ideas of electron-phonon interactions so as to include discussions of Stokes' shifts and exchange interactions etc.¹⁰ In order to study the EET dynamics of the molecular system embedded in condensed media, the environmental effect should be taken into account. Since molecules in solvents experience constantly changing intermolecular interactions, the time-dependent solute-solvent interactions cause time-dependent fluctuations of the eigenstates and eigenvalues of the molecules of interest. This can arise because identical molecules have different local environments in media. As a consequence, in our case, we have considered the environmental effect on the excitation energy migration process in which the energy fluctuations through the system-bath interactions are the main contributions to the population transfer between the eigenstates. Sim has developed the on-the-fly filtered propagator functional (OPPF) path integral formalism,^{11,12} that is based on the Feynman and Vernon's influence functional approach on a system coupled to a bath.¹³⁻¹⁵ By iteratively propagating in real-time, the reduced density matrix of the system of interest is calculated, which provides the time-evolution of the site population in the donor and acceptor state and, in turn, the EET rate constant. In this study, the path integral method is used to explore the environmental effect including solvent dynamics and polarization that affect the dynamics of the EET process within the linear geometry of ZnA ($n = 1, 2, 4, 6, 12,$ and 24) system.

This article is organized as follows: in Section 2, we discuss the OPFP path integral method in which important pathways contributing to the EET significantly are filtered on-the-fly and are integrated to provide numerically accurate site population over time. In Section 3, the time evolution of site population of ZnA systems at various number of donor units is evaluated. In order to explore the environmental effect of the total system, the parameters for spectral density are determined such that the tight-binding model system can reproduce the experimentally observed transfer rate constants. Concluding remarks are followed in Section 4.

Methodology

To model the EET processes in the ZnA system that is composed of strongly coupled n donor units and a single acceptor unit, the system is represented in terms of $(n+1)$ electronic states involved in the EET. Within the tight-binding system-bath Hamiltonian model,¹⁶ in which each site in the system represents a local exciton state, the system Hamiltonian has an $(n+1) \times (n+1)$ matrix form

$$\mathbf{H}_s = \begin{pmatrix} 0 & V_{DD} & 0 & \cdots & 0 \\ V_{DD} & 0 & V_{DD} & \cdots & \vdots \\ 0 & V_{DD} & \ddots & & 0 \\ \vdots & \vdots & & 0 & V_{DA} \\ 0 & \cdots & 0 & V_{DA} & E_{DA} \end{pmatrix} \quad (1)$$

where V_{DD} and V_{DA} are the donor-donor and donor-acceptor coupling constants, respectively, and E_{DA} is the energy difference between the donor and acceptor electronic states. Schematic diagram for the system Hamiltonian is drawn in Scheme 2. While the interactions between the donor S_1 states are rather strong ($V_{DD} = 570 \text{ cm}^{-1}$), the donor-acceptor coupling constant is weak ($V_{DA} = 29 \text{ cm}^{-1}$).^{6,8} From the absorption spectra of ZnA, the energy difference between the donor and acceptor is evaluated as $E_{DA} = -1600 \text{ cm}^{-1}$.⁶ The center-to-center distance between the acceptor and the nearest donor is 12.7 \AA and the donor-donor distance is 8.4 \AA .

Since the EET dynamics was measured in solution phase, bath should be included to mimic dissipative environment. While the bath consists of Q explicit harmonic modes, a weak system-bath interaction is assumed within the linear response limit. The total Hamiltonian is written as

$$H = H_s(s) + \sum_{j=1}^Q \left\{ \frac{1}{2} M_j \dot{x}_j^2 + \frac{1}{2} M_j \omega_j^2 x_j^2 \right\} - \sum_{j=1}^Q c_j x_j \sum_{k=1}^{n+1} \tilde{s}_k |u_k\rangle \langle u_k| \quad (2)$$

where $|u_k\rangle$ stands for an electronic state with corresponding grid point \tilde{s}_k while x_j is the j^{th} bath mode coordinate that is coupled to the system with a coupling constant c_j .

In order to describe the EET dynamics, it is necessary to evaluate the time-evolution of the reduced density matrix, defined as

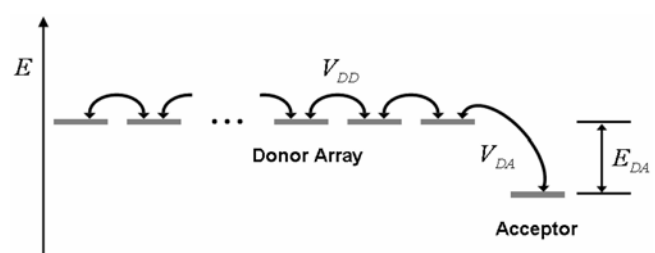
$$\tilde{\rho}(t) = \text{Tr}_b [e^{-iHt/\hbar} \rho(0) e^{-iHt/\hbar}]. \quad (3)$$

Diagonal elements of the reduced density matrix represent the population relaxation of the electronic states. In Eq. (3), Tr_b denotes the trace with respect to all the degrees of freedom of the bath. $\rho(0)$ is the initial density matrix of the system and bath in thermal equilibrium.

Following Feynman and Vernon's influence functional formalism, discretization of paths in time rewrites Eq. (3) as a multi-dimensional summation of the product of the system propagator and the influence functional

$$\tilde{\rho}(t) = \sum_i^{L_{tot}} \mathbf{S}(\Gamma_i^{(N)}) \mathbf{I}(\Gamma_i^{(N)}), \quad (4)$$

where the path from time 0 to t is discretized into $\Delta t = t/N$. $\Gamma_i^{(N)}$ is a path segment from time 0 to $N\Delta t$ that belongs to



Scheme 2. Schematic diagram of the tight-binding system model of ZnA systems.

the i^{th} path. The summation in Eq. (4) runs over all possible paths connecting $(n+1)$ electronic states leading to $L_{\text{tot}} = (n+1)^{2N}$. The system propagator S accounts for the transport within the system in the absence of a bath such that

$$S(\tilde{s}_{k_0^\pm}, \dots, \tilde{s}_{k_N^\pm}) = \langle u_{k_0^\pm} | \tilde{\rho}(0) | u_{k_0^\pm} \rangle \times \prod_{j=1}^{N-1} S_{k_j}(\tilde{s}_{k_j^\pm}, \tilde{s}_{k_{j-1}^\pm}) \times S_{k_N}(\tilde{s}_{k_N^\pm}, \tilde{s}_{k_{N-1}^\pm}). \quad (5)$$

Here, $+$ ($-$) sign in subscripts depicts forward (backward) propagating path segments, therefore, $\tilde{s}_{k_j^+}$ ($\tilde{s}_{k_j^-}$) corresponds to a grid point at time $j\Delta t$ in the k^{th} forward (backward) path. One-dimensional forward and backward short-time propagator is defined as

$$S_{k_j} = \langle u_{k_j^\pm} | e^{-iH_s\Delta t/\hbar} | u_{k_{j-1}^\pm} \rangle \langle u_{k_{j-1}^\pm} | e^{iH_s\Delta t/\hbar} | u_{k_j^\pm} \rangle. \quad (6)$$

On the other hand, the influence functional I arises from the coupling to the environment, and for the harmonic bath, it has the closed form as

$$I(\tilde{s}_{k_0^\pm}, \dots, \tilde{s}_{k_N^\pm}; t) = \exp\left\{-\frac{1}{\hbar} \sum_{j=0}^N \sum_{j'=0}^j (\tilde{s}_{k_j^\pm} - \tilde{s}_{k_{j'}^\pm})(\eta_{k_j k_{j'}} \tilde{s}_{k_j^\pm} - \eta_{k_j k_{j'}}^* \tilde{s}_{k_{j'}^\pm})\right\}, \quad (7)$$

$$= \prod_{j=0}^{N-1} \prod_{j'=0}^j I_{k_j k_{j'}}(\tilde{s}_{k_j^\pm}, \tilde{s}_{k_{j'}^\pm}) \times \prod_{j'=0}^N I_{k_N k_{j'}}(\tilde{s}_{k_N^\pm}, \tilde{s}_{k_{j'}^\pm})$$

where the influence interaction between $j\Delta t$ and $j'\Delta t$ time points is

$$I_{k_j k_{j'}} = \exp\left\{-\frac{1}{\hbar} (\tilde{s}_{k_j^\pm} - \tilde{s}_{k_{j'}^\pm})(\eta_{k_j k_{j'}} \tilde{s}_{k_j^\pm} - \eta_{k_j k_{j'}}^* \tilde{s}_{k_{j'}^\pm})\right\}. \quad (8)$$

Expressions for the influence coefficients $\eta_{kk'}$ can be found in Ref. 17.

In order to avoid redundant calculations of memory interactions, the OFPF important path integral approach rewrites Eq. (4) as a sum of products of history \mathcal{T} and propagator functional \mathcal{P}^e ,⁶

$$\tilde{\rho}(t) = \sum_i^{L_{\text{tot}}} \mathcal{T}(\Gamma_i^{(N-1)}) \mathcal{P}^e(\Gamma_i^{(N)}). \quad (9)$$

For the density matrix at the present time t , the history term involves interactions between the past time points (from 0 to $t - \Delta t$) independent of t ,

$$\mathcal{T}(\Gamma_i^{(N-1)}) = \langle k_0^+ | \tilde{\rho}(0) | k_0^- \rangle \times \prod_{j=1}^{N-1} S_{k_j} \prod_{j=0}^{N-1} \prod_{j'=0}^j I_{k_j k_{j'}}, \quad (10)$$

while the propagator functional includes the interactions between the present and the past time points

$$\mathcal{P}^e(\Gamma_i^{(N)}) = S_{k_N} \times \prod_{j=0}^N I_{k_N k_j}. \quad (11)$$

Consequently, a significant amount of redundant calculations for the history path segments can be avoided by storing each configuration and corresponding weight, nonetheless the number of total configurations increases exponentially as $(n+1)^{2N}$. This exponential scaling is resolved by utilizing the rapid dissipation of the nonlocal interaction strength beyond the bath memory time τ_m ; it is sufficient to include only $(n+1)^{2N_m}$ configurations for the times $t > \tau_m$ without losing numerical accuracy, leading to the saturation of the number of paths to be included in the path integration.⁸ Furthermore, the OFPF important path integration performs on-the-fly filtering such that, up to $t = \tau_m$, the number of paths increases linearly with the propagation time.

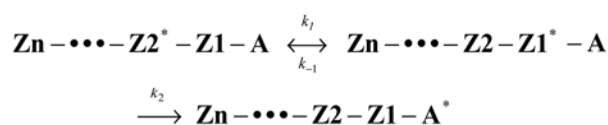
Discussion

To describe the energy transfer dynamics in ZnA, we first adopted the Förster mechanism by assuming the donor array as one single chromophore, resulting in^{18,19}

$$k = \frac{8.8 \times 10^{-25} \kappa^2 \Phi J}{n^4 R^6 \tau} \quad (12)$$

$$J = \int F(\nu) \varepsilon(\nu) \nu^{-4} d\nu \quad (13)$$

where n is the refractive index of the solvent, R is the center-to-center distance between donor and acceptor, Φ is the fluorescence quantum yield of donor, τ is the fluorescence lifetime of donor, and κ is a dipole-dipole orientation factor. Also, J is the spectral overlap integral. The Förster energy transfer rate constants are estimated to be $(5.2 \text{ ps})^{-1}$ for Z1A, $(6.9 \text{ ps})^{-1}$ for Z2A, $(20 \text{ ps})^{-1}$ for Z3A, and $(160 \text{ ps})^{-1}$ for Z6A, $(2300 \text{ ps})^{-1}$ for Z12A, and $(49000 \text{ ps})^{-1}$ for Z24A, respectively, which are really remote from the experimentally observed values. These slow energy transfer rates stem mainly from the intermolecular distance (R) term, that means, the assumption that meso-meso linked porphyrin array is one single chromophore is not appropriate. Thus, we considered each porphyrin moiety in Zn as one single chromophore. In this type of random walk model, we took a matrix-formulated eigenvalue/eigenvector approach implemented by Donohoe and coworkers, using empirical data to predict the quantum efficiency.^{20,21} In our case, the energy transfer scheme was given as the following, assuming that the absorption characteristics of each porphyrin unit in the donor are identical.



The model yields pseudo-first-order production since k_1 would be much faster than k_2 , which is predictable from the fact that the excitation energy hopping rate in Zn is estimated to be $(\sim 0.2 \text{ ps})^{-1}$ in the previous femtosecond transient absorption anisotropy decay of Zn and the energy

transfer rate from photoexcited Zn(II) porphyrin to free-base porphyrin in the *meso-meso* phenylene linked porphyrin heterodimer is evaluated to be (~ 3 ps) $^{-1}$. Based on the above assumptions, we can make following equation,

$$\frac{d\mathbf{A}^*}{dt} = k_2 \mathbf{Z} \mathbf{I}^* \approx \frac{k_2}{n} \quad (14)$$

where \mathbf{A}^* and $\mathbf{Z} \mathbf{I}^*$ represent the local excited state of A and ZI, respectively. Although the energy transfer rates calculated from Eq. (14) are not so outrageous compared with the experimental values evaluated from the transient absorption measurements, they are still unsatisfactory.

To improve the correlation between the experimental values and our simulation on the EET rates in the ZnA system, we include time-dependent fluctuations of the eigenstates and eigenvalues of the ZnA system using a dissipative bath that is coupled to the system. Bath properties influencing the dynamics of the system are contained in the coupling constants $\{c_j\}$ in Eq. (2). Potential parameters of porphyrin arrays can be easily obtained from experiments; however, information regarding the system-bath interaction is unavailable. Since the bath is composed of semi-infinite number of modes, it is advantageous to use the spectral density instead of explicit coupling constants. With harmonic bath modes, the spectral density is defined as

$$J(\omega) = \frac{\pi}{2} \sum_{j=1}^Q \frac{c_j^2}{m_j \omega_j} \delta(\omega - \omega_j). \quad (15)$$

The system-bath interaction is described by the ohmic spectral density with the characteristic frequency of ω_c and the Kondo parameter ξ ²²

$$J(\omega) = \frac{\pi \hbar}{2} \xi \omega \exp(-\omega/\omega_c). \quad (16)$$

The more quantitative solvent characteristic, "solvent reorganization energy, λ " is correlated with the spectral density through the following relationship:

$$\lambda = \frac{1}{\pi} \int_0^\infty d\omega \frac{J(\omega)}{\omega} \times d_{DA}^2 \quad (17)$$

where d_{DA} is the distance between the donor and acceptor. By substituting Eq. (13) and performing the integration, we obtain the relationship between the Kondo parameter and the solvent reorganization energy:

$$\xi = \frac{2\lambda}{\hbar \omega_c d_{DA}^2}. \quad (18)$$

Since the spectral density represents the system-bath interaction in the frequency domain, it has the maximum intensity at the cutoff frequency and the overall intensity increases with the bath friction, *i.e.*, the Kondo parameter. Although the overall intensity increases with the solvent reorganization energy, the position of the maximum intensity remains unchanged as shown in Figure 1(a). On the other hand, the position of the maximum intensity is shifted to

higher frequency with the cutoff frequency as shown in Figure 1(b).

The trace of the bath degrees of freedom in Eq. (3) leads to a non-Markovian dynamics in which the integrated bath modes are transformed to memory in the system dynamics.²³ Since the bath memory dissipates to zero after a finite time, non-local interactions between the time points that are separated more than the bath memory time, τ_m , can be neglected in path integration without losing numerical accuracy. In general, the cutoff frequency governs the duration of the system-bath interaction and the reorganization energy affects the interaction strength according to Eq. (15).

Let us consider the simplest system, ZIA, which comprises a single donor porphyrin unit and a single acceptor unit. The two-state tight binding model is thus used according to Eq. (1),

$$\mathbf{H}_s = \begin{pmatrix} 0 & V_{DA} \\ V_{DA} & E_{DA} \end{pmatrix}. \quad (19)$$

Although the spectral density for the energy transfer in

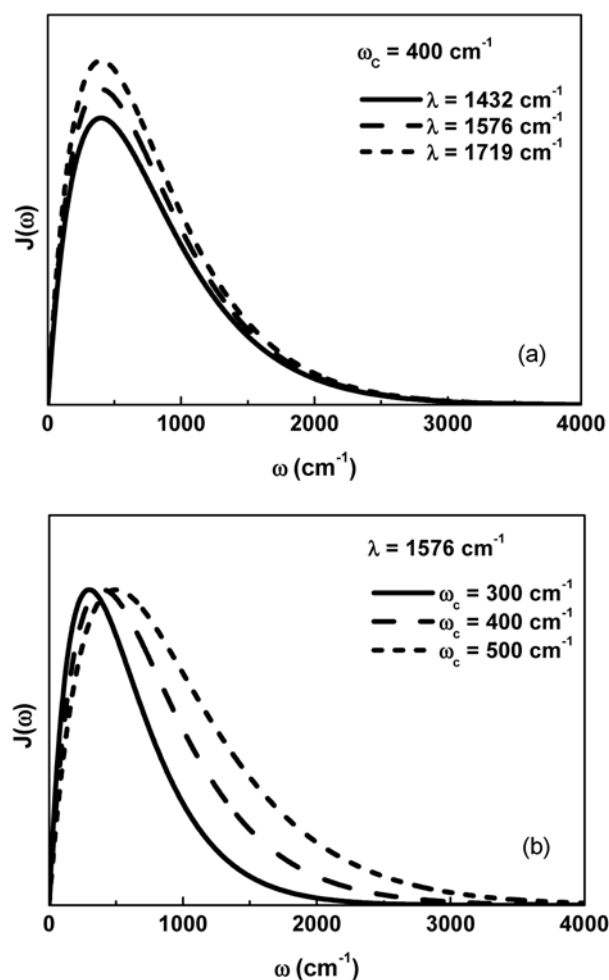


Figure 1. Ohmic spectral densities at (a) constant cutoff frequency $\omega_c = 400$ cm^{-1} and (b) constant reorganization energy $\lambda = 1576$ cm^{-1} .

porphyrin arrays in toluene is unavailable, the bath cutoff frequency of the porphyrin-quinone compound in acetonitrile has been reported as 400 cm^{-1} using molecular dynamics simulations.²⁴ In addition, the solvent reorganization energy of the porphyrin-quinone in toluene has been estimated to be $1900\text{--}2200\text{ cm}^{-1}$.²⁵

Optimization of the spectral density for the EET process in ZnA requires searching for the parameters by varying the cutoff frequency as $400 \leq \omega_c \leq 500\text{ cm}^{-1}$ and the solvent reorganization energy as $1000 \leq \lambda \leq 2500\text{ cm}^{-1}$. At a given cutoff frequency, the bath memory time is estimated upon the convergence of the site population as elongating the path segments in which the memory interactions among time points are fully taken into account. Figure 2 presents the acceptor population rise over time at $\omega_c = 500\text{ cm}^{-1}$ and $\lambda = 1790\text{ cm}^{-1}$. It is clear that the acceptor population converges at $\tau_m = 22\text{ fs}$. The bath response function in the inset confirms that the choice of $\tau_m = 22\text{ fs}$ is appropriate.

The propagation time step is also decided, which could yield numerically converging results. By keeping τ_m as the predetermined value of 22 fs , the convergence of acceptor population is examined by comparing the results obtained by $\Delta t = 0.5, 1, 2\text{ fs}$. In Figure 3, the acceptor populations for $\Delta t \leq 1\text{ fs}$ become indistinguishable. Therefore, when the environment is described by the spectral density parameters $\omega_c = 500\text{ cm}^{-1}$ and $\lambda = 1790\text{ cm}^{-1}$, the path integration condition is set as $\Delta t = 1\text{ fs}$ and $\tau_m = 22\text{ fs}$. Following the same procedure, the bath memory time is estimated to be 40 fs when the spectral cutoff frequency is 400 cm^{-1} . $\Delta t = 1\text{ fs}$ is small enough to reproduce the converged population. For the Z1A system, the spectral density parameters of (ω_c, λ) as $(400\text{ cm}^{-1}, 1576\text{ cm}^{-1})$ and $(500\text{ cm}^{-1}, 1790\text{ cm}^{-1})$ give rise to the experimental energy transfer rate constant of $(2.5\text{ ps})^{-1}$.

For the Z2A system, there are two donor porphyrin units and a single acceptor unit and the system Hamiltonian has a 3×3 matrix form,

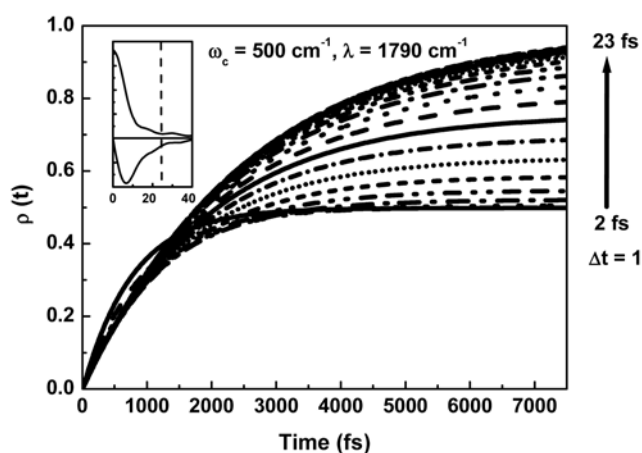


Figure 2. Site population of the acceptor as a function of the bath memory time included from 1 fs to 23 fs . The propagation time step is chosen to be 1 fs . Environment is described by the ohmic spectral density with the cutoff frequency $\omega_c = 500\text{ cm}^{-1}$ and the solvent reorganization energy $\lambda = 1790\text{ cm}^{-1}$.

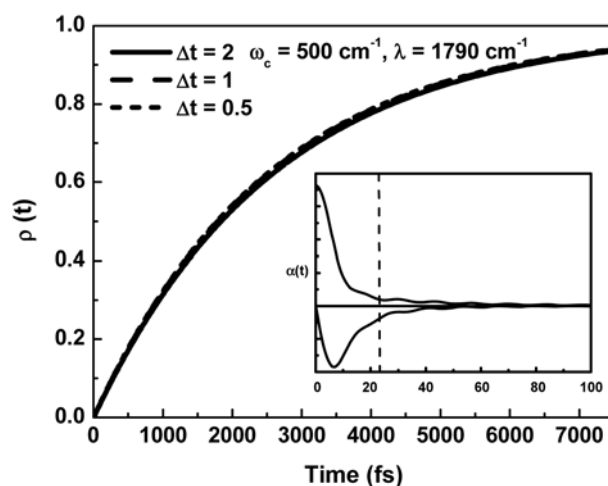


Figure 3. Site population of the acceptor as a function of the propagation time step. Bath memory time is chosen to be $\tau_m = 22\text{ fs}$. Environment is described by the ohmic spectral density with the cutoff frequency $\omega_c = 500\text{ cm}^{-1}$ and the solvent reorganization energy $\lambda = 1790\text{ cm}^{-1}$.

$$\mathbf{H}_s = \begin{pmatrix} 0 & V_{DD} & 0 \\ V_{DD} & 0 & V_{DA} \\ 0 & V_{DA} & E_{DA} \end{pmatrix}. \quad (20)$$

The initial condition is chosen such that the donor porphyrin unit closest to the acceptor is excited while the other porphyrin unit is in the ground state. While the energy can only transfer from the single donor unit to the acceptor in Z1A system, for larger systems, starting from Z2A, the excitation energy hops between excited electronic states, and is eventually trapped in the acceptor. As shown in Figure 4, extremely rapid equilibration with the time constant of $\sim 0.2\text{ ps}$ is achieved within the two donor states in Z2A due to the strong interaction of V_{DD} . Such behavior is expected to occur

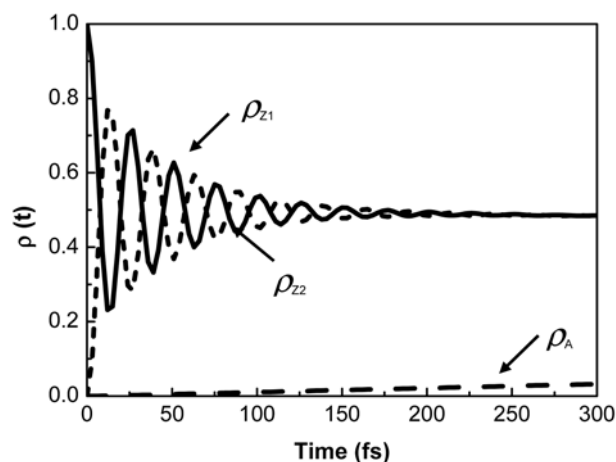


Figure 4. Site population of the three electronic states of Z2A system. Environment is described by the ohmic spectral density with the cutoff frequency $\omega_c = 500\text{ cm}^{-1}$ and the solvent reorganization energy $\lambda = 1790\text{ cm}^{-1}$. Solid line corresponds to the Z1 donor, dashed line to the Z2 donor, and the long-dashed line is the acceptor.

in a longer donor array as well. Therefore, for ZnA system with $n > 1$, n porphyrin units can be modeled as one coherently coupled donor state, acceptable when n is smaller than the coherent length L , which interacts with the acceptor such that the system Hamiltonian is reduced to a 2×2 matrix given as

$$\mathbf{H}_s = \begin{pmatrix} 0 & V_n \\ V_n & E_{DA} \end{pmatrix} \quad (21)$$

with the effective coupling constant between the effective donor and the acceptor when n is less than L in the following form⁶

$$V_n = V_{DA} \sqrt{\frac{2}{n+1}} \sum_{k=1}^n \sin\left(\frac{\pi}{n+1}k\right) \left(\frac{R_1}{R_k}\right)^3, \text{ for } n \leq L, \quad (22)$$

where n is the number of porphyrin units in the donor array and V_{DA} represents the coupling strength between donor and acceptor in ZIA. R_k is the center-to-center distance between the acceptor and the k^{th} porphyrin unit in the donor array while R_1 is that of the nearest porphyrin unit from the acceptor. On the other hand, as a finite number of porphyrin moieties are coherently coupled up to a certain length L , the effective coupling for the long arrays should be modified as follows.

$$V_n = \frac{V_L}{\sqrt{N-L+1}}, \quad \text{for } n > L. \quad (24)$$

By employing the optimal spectral densities chosen for the ZIA system and the effective two-state system Hamiltonian in Eq. (21), we have carried out the OFPF path integral simulation on the effective two-state tight binding Hamiltonian to estimate the energy transfer rates for the ZnA

Table 1. Energy transfer rate constants at $\omega_c = 400 \text{ cm}^{-1}$, $\lambda = 1576 \text{ cm}^{-1}$. Units are in $(\text{ps})^{-1}$. Lx indicates that the rate constants are evaluated assuming the coherent length $L = x$

	Exp.	L1	L2	L3	L4	L5	L6
Z1A	2.5 ± 0.1	2.4	2.4	2.4	2.4	2.4	2.4
Z2A	3.3 ± 0.2	4.5	3.2	3.2	3.2	3.2	3.2
Z3A	5.5 ± 0.5	6.9	6.2	5.0	5.0	5.0	5.0
Z6A	21 ± 2	14	17	20	22	22	17
Z12A	63 ± 5	28	35	49	69	98	120
Z24A	108 ± 7	59	80	120	130	210	280

Table 2. Energy transfer rate constants at $\omega_c = 500 \text{ cm}^{-1}$, $\lambda = 1790 \text{ cm}^{-1}$. Units are in $(\text{ps})^{-1}$. Lx indicates that the rate constants are evaluated assuming the coherent length $L = x$

	Exp.	L1	L2	L3	L4	L5	L6
Z1A	2.5 ± 0.1	2.6	2.6	2.6	2.6	2.6	2.6
Z2A	3.3 ± 0.2	5.0	3.5	3.5	3.5	3.5	3.5
Z3A	5.5 ± 0.5	7.6	6.8	5.5	5.5	5.5	5.5
Z6A	21 ± 2	15	18	22	24	24	18
Z12A	63 ± 5	31	38	54	78	110	140
Z24A	108 ± 7	64	89	140	160	220	300

system ($n = 2, 4, 6, 12$ and 24) as a function of the coherent length L . By varying the coherent length from 1 to 6, in Tables 1 and 2, the energy transfer rate constants are compared with sets of the spectral density parameters (ω_c, λ) as $(400 \text{ cm}^{-1}, 1576 \text{ cm}^{-1})$ and $(500 \text{ cm}^{-1}, 1790 \text{ cm}^{-1})$, respectively. We observed an excellent agreement between the simulated and experimentally determined rate constants especially when the spectral density parameters (ω_c, λ) are $(400 \text{ cm}^{-1}, 1576 \text{ cm}^{-1})$ and L is equal to 4. The coherent length $L = 4$ obtained in our EET simulation also matches well with the radiative coherent length of $L \sim 4$ obtained in the previous work from the plot of the natural radiative lifetimes as a function of porphyrin units in Zn arrays.²⁶ This feature indicates that the excited state of the tightly bound porphyrin arrays should be a coupled state covering a number of porphyrins coherently. Overall, our path integral method has proven to be a suitable tool to simulate the EET processes occurring in energy donor-acceptor system composed of porphyrin assemblies.

Concluding Remarks

We have applied the real-time OFPF path integral formalism to the simulation of the EET processes within ZnA systems composed of 5,15-bisphenylethynylated porphyrin unit as the energy acceptor and directly *meso-meso* linked Zn(II) porphyrin array as the energy donor. Regarding the porphyrin donor array as coherently coupled one, the system is modeled with the two-state tight binding donor-acceptor system coupled to a harmonic bath that is described by an ohmic spectral density. Accurate real-time quantum mechanical simulations of the time-evolution of the site population of ZnA ($n = 1, 2, 4, 6, 12$ and 24) systems have been performed and the experimentally observed EET rate constants were reproduced excellently. Conclusively, all donor-acceptor systems illustrate highly-efficient molecular photonic wire due to large excitonic interactions arising from a close proximity and a lack of energy sink owing to well-defined orthogonal geometry along the arrays.

In this work, the coherent length was determined based on the simulated dynamics performed on the system-bath Hamiltonian. Dynamical characteristics of the decoherence, *i.e.*, the dephasing time, is absent in the present study due to the use of the effective model. The path integral methodology is general to be employed in various EET problems. In particular, it is straightforward to extend the methodology to multi-state systems in which each site represents an explicit local exciton state. Off-diagonal elements of the reduced density matrix provide details of the dephasing time and direct measurement of the decoherence strength. Investigation of EET using quantum mechanical simulations should be crucial to understanding the energy transfer mechanism in various molecular photonic systems and devices where energy transfer process characterizes their properties and functions. Aforementioned multi-state energy transfer simulations are under progress and will be presented in future publications.

Acknowledgment. This work was financially supported by the KOSEF (Korea Science and Engineering Foundation) through GRANT R04-2004-000-10009-0 (ES) and the National Creative Research Initiatives Program (DK).

References

1. Sundstrom, V.; Pullerits, T.; Grondelle, R. *J. Phys. Chem. B* **1999**, *103*, 2327.
 2. Warshel, A.; Parson, W. W. *J. Am. Chem. Soc.* **1987**, *109*, 6143.
 3. Knapp, E. W.; Fischer, S. F.; Zinth, W.; Sander, M.; Kaiser, W.; Deisenhofer, J.; Michel, H. *Proc. Natl. Acad. Sci. USA* **1985**, *82*, 8463.
 4. Makri, N.; Sim, E.; Topaler, M.; Makarov, D. E. *Proc. Natl. Acad. Sci. USA* **1996**, *93*, 3926.
 5. Sim, E.; Makri, N. *J. Phys. Chem.* **1997**, *101*, 5446.
 6. Aratani, N.; Cho, H. S.; Ahn, T. K.; Cho, S.; Kim, D.; Sumi, H.; Osuka, A. *J. Am. Chem. Soc.* **2003**, *125*, 9668.
 7. Song, N. W.; Cho, H. S.; Yoon, M. C.; Aratani, N.; Osuka, A.; Kim, D. *Bull. Korean Chem. Soc.* **2002**, *23*, 271.
 8. Kim, Y. H.; Jeong, D. H.; Kim, D.; Jeoung, S. C.; Cho, H. S.; Kim, S. K.; Aratani, N.; Osuka, A. *J. Am. Chem. Soc.* **2001**, *123*, 76.
 9. Forster, T. *Discuss. Faraday Soc.* **1959**, *27*, 7.
 10. Dexter, D. L. *J. Chem. Phys.* **1953**, *21*, 836.
 11. Sim, E. *J. Chem. Phys.* **2001**, *115*, 4450.
 12. Sim, E. *J. Phys. Chem. B* **2004**, *108*, 19093.
 13. Feynman, R. P.; Vernon, F. L. *Ann. Phys.* **1963**, *24*, 118.
 14. Makri, N.; Makarov, D. E. *J. Chem. Phys.* **1995**, *102*, 4600; *102*, 4611.
 15. Sim, E.; Makri, N. *Chem. Phys. Lett.* **1996**, *249*, 224.
 16. Leggett, A. J.; Chakravarty, S.; Dorsey, A. T.; Fisher, M. P. A.; Garg, A.; Zwirger, W. *Rev. Mod. Phys.* **1987**, *59*, 1.
 17. Sim, E.; Makri, N. *Comput. Phys. Commun.* **1997**, *99*, 335.
 18. Förster, T. *Ann. Phys.* **1948**, *2*, 55.
 19. Förster, T. *Discuss. Faraday Soc.* **1959**, *27*, 7.
 20. van Patten, P. G.; Shreve, A. P.; Lindsey, J. S.; Donohoe, R. J. *Phys. Chem. B* **1998**, *102*, 4209.
 21. Cho, H. S.; Jeong, D. H.; Yoon, M.-C.; Kim, Y. H.; Kim, Y.-R.; Kim, D.; Jeoung, S. C.; Kim, S. K.; Aratani, N.; Shimori, H.; Osuka, A. *J. Phys. Chem. A* **2001**, *105*, 4200.
 22. Winterstetter, M. *Phys. Rev. E* **1999**, *60*, 203.
 23. Weiss, U. *Quantum Dissipative Systems*; World Scientific: New Jersey, 1993.
 24. Hayashi, S.; Kato, S. *J. Phys. Chem. A* **1998**, *102*, 3333.
 25. Perng, B.; Newton, M. D.; Raineri, F. O.; Friedman, H. L. *J. Chem. Phys.* **1996**, *104*, 7177.
 26. Ahn, T. K.; Yoon, Z. S.; Hwang, I.-W.; Lim, J. K.; Rhee, H.; Joo, T.; Sim, E.; Kim, S. K.; Aratani, N.; Osuka, A.; Kim, D. *J. Phys. Chem. B* **2005**, *109*, 11223.
-